Disordered nanostructures by hole-mask colloidal lithography for advanced light trapping in silicon solar cells

Disordered nanostructures by hole-mask colloidal lithography for advanced light trapping in silicon solar cells

Christos Trompoukis,[1,2,6,7,9,*] Inès Massiot,[3,9] Valérie Depauw,[1] Ounsi El Daif,[1,8] Kidong Lee,[4] Alexandre Dmitriev,[3] Ivan Gordon,[1] Robert Mertens,[1] and Jef Poortmans[1,2,5]

[1]*imec, Kapeldreef 75, B-3001 Leuven, Belgium*
[2]*KU Leuven, Departement Elektrotechniek – ESAT, Kasteelpark Arenberg 10, B-3001 Leuven, Belgium*
[3]*Chalmers University of Technology, Department of Applied Physics, SE-412 96 Gothenburg, Sweden*
[4]*Obducat Technologies AB, Scheelevägen 2, 223 63 Lund, Sweden*
[5]*University of Hasselt, Martelarenlaan 42, 3500 Hasselt, Belgium*
[6]*Currently with Ghent University, Department of Information Technology, Photonics Research Group, Sint-Pietersnieuwstraat 41, B-9000 Gent, Belgium*
[7]*Currently with KU Leuven, Centre for Surface Chemistry and Catalysis, Celestijnenlaan 200F Leuven Chem & Tech post box 2461, B-3001 Leuven, Belgium*
[8]*Currently with Qatar Environment and Energy Research Institute (QEERI) 5825 Doha, Qatar*
[9]*These authors contributed equally to this work*
[*]*christos.trompoukis@ugent.be*

Abstract: We report on the fabrication of disordered nanostructures by combining colloidal lithography and silicon etching. We show good control of the short-range ordered colloidal pattern for a wide range of bead sizes from 170 to 850 nm. The inter-particle spacing follows a Gaussian distribution with the average distance between two neighboring beads (center to center) being approximately twice their diameter, thus enabling the nanopatterning with dimensions relevant to the light wavelength scale. The disordered nanostructures result in a lower integrated reflectance (8.1%) than state-of-the-art random pyramid texturing (11.7%) when fabricated on 700 μm thick wafers. When integrated in a 1.1 μm thin crystalline silicon slab, the absorption is enhanced from 24.0% up to 64.3%. The broadening of resonant modes present for the disordered nanopattern offers a more broadband light confinement compared to a periodic nanopattern. Owing to its simplicity, versatility and the degrees of freedom it offers, this potentially low-cost bottom-up nanopatterning process opens perspectives towards the integration of advanced light-trapping schemes in thin solar cells.

OCIS codes: (350.6050) Solar energy; (310.6628) Subwavelength structures, nanostructures; (310.6845) Thin film devices and applications; (040.5350) Photovoltaic.

References and links

1. J. D. Joannopoulos, S. G. Johnson, J. N. Winn, and R. D. Meade, *Photonic Crystals: Molding the Flow of Light* (Princeton University, 2008).
2. P. Sheng, A. N. Bloch, and R. S. Stepleman, "Wavelength-selective absorption enhancement in thin-film solar cells," Appl. Phys. Lett. **43**(6), 579–581 (1983).
3. A. Mellor, I. Tobias, A. Marti, M. J. Mendes, and A. Luque, "Upper limits to absorption enhancement in thick solar cells using diffraction gratings," Prog. Photovolt. Res. Appl. **19**(6), 676–687 (2011).
4. K. X. Wang, Z. Yu, V. Liu, Y. Cui, and S. Fan, "Absorption enhancement in ultrathin crystalline silicon solar cells with antireflection and light-trapping nanocone gratings," Nano Lett. **12**(3), 1616–1619 (2012).
5. Z. Yu, A. Raman, and S. Fan, "Nanophotonic light-trapping theory for solar cells," Appl. Phys., A Mater. Sci. Process. **105**(2), 329–339 (2011).
6. E. Yablonovitch and G. D. Cody, "Intensity enhancement in textured optical sheets for solar cells," IEEE Trans. Electron. Dev. **29**(2), 300–305 (1982).

#251986 Received 15 Oct 2015; revised 25 Nov 2015; accepted 29 Nov 2015; published 11 Dec 2015

7. A. Goetzberger, “Optical confinement in thin Si solar cells by diffuse back reflectors,” Proceedings of the 15th IEEE Photovoltaic Specialists Conference, Kissimmee, FL, pp. 867–870, (1981).
8. H. Jansen, M. de Boer, R. Legtenberg, and M. Elwenspoek, “The black silicon method: a universal method for determining the parameter setting of a fluorine-based reactive ion etcher in deep silicon trench etching with profile control,” J. Micromech. Microeng. **5**(2), 115–120 (1995).
9. S. Koynov, M. S. Brandt, and M. Stutzmann, “Black nonreflecting silicon surfaces for solar cells,” Appl. Phys. Lett. **88**(20), 203107 (2006).
10. X. Liu, P. R. Coxon, M. Peters, B. Hoex, J. M. Cole, and D. J. Fray, “Black silicon: fabrication methods, properties and solar energy applications,” Energy Environ. Sci. **7**(10), 3223–3263 (2014).
11. A. Bett, J. Eisenlohr, O. Höhn, B. Bläsi, J. Benick, P. Repo, H. Savin, J. C. Goldschmidt, and M. Hermle, “Front side antireflection concepts for silicon solar cells with diffractive rear side structures,” 29th European Photovoltaic Solar Energy Conference and Exhibition 2014 Amsterdam, The Netherlands, pp. 987–991.
12. K. Vynck, M. Burresi, F. Riboli, and D. S. Wiersma, “Photon management in two-dimensional disordered media,” Nat. Mater. **11**(12), 1017–1022 (2012).
13. A. Bozzola, M. Liscidini, and L. C. Andreani, “Broadband light trapping with disordered photonic structures in thin-film silicon solar cells,” Prog. Photovolt. Res. Appl. **22**, 1237–1245 (2014).
14. R. Peretti, G. Gomard, L. Lalouat, C. Seassal, and E. Drouard, “Absorption control in pseudodisordered photonic-crystal thin films,” Phys. Rev. A **88**(5), 053835 (2013).
15. E. R. Martins, J. Li, Y. Liu, J. Zhou, and T. F. Krauss, “Engineering gratings for light trapping in photovoltaics: the supercell concept,” Phys. Rev. B **86**(4), 041404 (2012).
16. A. Oskooi, P. A. Favuzzi, Y. Tanaka, H. Shigeta, Y. Kawakami, and S. Noda, “Partially disordered photonic crystal thin films for enhanced and robust photovoltaics,” Appl. Phys. Lett. **100**(18), 181110 (2012).
17. J. Muller, A. Herman, A. Mayer, and O. Deparis, “A fair comparison between ultrathin crystalline-silicon solar cells with either periodic or correlated disorder inverted pyramid textures,” Opt. Express **23**(11), A657–A670 (2015).
18. A. Mavrokefalos, S. E. Han, S. Yerci, M. S. Branham, and G. Chen, “Efficient light trapping in inverted nanopyramid thin crystalline silicon membranes for solar cell applications,” Nano Lett. **12**(6), 2792–2796 (2012).
19. S. Y. Chou, P. R. Krauss, and P. J. Renstrom, “Imprint lithography with 25-nanometer resolution,” Science **272**(5258), 85–87 (1996).
20. P. Pieranski, “Two-dimensional interfacial colloidal crystals,” Phys. Rev. Lett. **45**(7), 569–572 (1980).
21. G. Zhang and D. Wang, “Colloidal lithography--the art of nanochemical patterning,” Chem. Asian J. **4**(2), 236–245 (2009).
22. P. Gao, J. He, S. Zhou, X. Yang, S. Li, J. Sheng, D. Wang, T. Yu, J. Ye, and Y. Cui, “Large-area nanosphere self-assembly by a micro-propulsive injection method for high throughput periodic surface nanotexturing,” Nano Lett. **15**(7), 4591–4598 (2015).
23. H. Fredriksson, Y. Alaverdyan, A. Dmitriev, C. Langhammer, D. S. Sutherland, M. Zach, and B. Kasemo, “Hole–mask colloidal lithography,” Adv. Mater. **19**(23), 4297–4302 (2007).
24. C. Trompoukis, O. El Daif, V. Depauw, I. Gordon, and J. Poortmans, “Photonic assisted light trapping integrated in ultrathin crystalline silicon solar cells by nanoimprint lithography,” Appl. Phys. Lett. **101**(10), 103901 (2012).
25. V. Depauw, Y. Qiu, K. Van Nieuwenhuysen, I. Gordon, and J. Poortmans, “Epitaxy-free monocrystalline silicon thin film: first steps beyond proof-of-concept solar cells,” Prog. Photovolt. Res. Appl. **19**(7), 844–850 (2011).
26. C. Trompoukis, I. Abdo, R. Cariou, I. Cosme, W. Chen, O. Deparis, A. Dmitriev, E. Drouard, M. Foldyna, E. G. Caurel, I. Gordon, B. Heidari, A. Herman, L. Lalouat, K.-D. Lee, J. Liu, K. Lodewijks, F. Mandorlo, I. Massiot, A. Mayer, V. Mijkovic, J. Muller, R. Orobtchouk, G. Poulain, P. Prod’Homme, P. R. Cabarrocas, C. Seassal, J. Poortmans, R. Mertens, O. E. Daif, and V. Depauw, “Photonic nanostructures for advanced light trapping in thin crystalline silicon solar cells,” Phys. Status Solidi **212**(1), 140–155 (2015).
27. www.obducat.com
28. T. Eriksson, S. Yamada, P. V. Krishnan, S. Ramasamy, and B. Heidari, “High volume nanoimprint lithography on III/V substrates: Imprint fidelity and stamp lifetime,” Microelectron. Eng. **88**(3), 293–299 (2011).
29. C. Trompoukis, O. El Daif, P. Pratim Sharma, H. Sivaramakrishnan Radhakrishnan, M. Debucquoy, V. Depauw, K. Van Nieuwenhuysen, I. Gordon, R. Mertens, and J. Poortmans, “Passivation of photonic nanostructures for crystalline silicon solar cells,” Prog. Photovolt. Res. Appl. **23**(6), 734–742 (2015).
30. P. Verdonck, A. Goodyear, R. D. Mansano, P. R. J. Barroy, and N. St. J. Braithwaite, “Importance of fluorine surface diffusion for plasma etching of silicon,” J. Vac. Sci. Technol. B **20**, 791–796 (2002).
31. H. Seidel and L. Csepregi, “Anisotropic etching of crystalline silicon in alkaline solutions,” J. Electrochem. Soc. **137**(11), 3612 (1990).
32. P. Hanarp, D. S. Sutherland, J. Gold, and B. Kasemo, “Control of nanoparticle film structure for colloidal lithography,” Colloids Surf. A Physicochem. Eng. Asp. **214**(1-3), 23–36 (2003).
33. P. Gao, H. Wang, Z. Sun, W. Han, J. Li, and J. Ye, “Efficient light trapping in low aspect-ratio honeycomb nanobowl surface texturing for crystalline silicon solar cell applications,” Appl. Phys. Lett. **103**(25), 253105 (2013).
34. A. Herman, C. Trompoukis, V. Depauw, O. El Daif, and O. Deparis, “Influence of the pattern shape on the efficiency of front-side periodically patterned ultrathin crystalline silicon solar cells,” J. Appl. Phys. **112**(11), 113107 (2012).

#251986 Received 15 Oct 2015; revised 25 Nov 2015; accepted 29 Nov 2015; published 11 Dec 2015

35. A. Bozzola, M. Liscidini, and L. C. Andreani, "Photonic light-trapping versus Lambertian limits in thin film silicon solar cells with 1D and 2D periodic patterns," Opt. Express **20**(S2), A224–A244 (2012).
36. C. Battaglia, C. M. Hsu, K. Söderström, J. Escarré, F.-J. Haug, M. Charrière, M. Boccard, M. Despeisse, D. T. L. Alexander, M. Cantoni, Y. Cui, and C. Ballif, "Light trapping in solar cells: can periodic beat random?" ACS Nano **6**(3), 2790–2797 (2012).
37. V. Depauw, I. Abdo, R. Boukhicha, R. Cariou, W. Chen, I. Cosme Bolanos, O. Deparis, H. Ding, A. Dmitriev, E. Drouard, O. El Daif, A. Fave, M. Foldyna, E. Garcia-Caurel, B. Heidari, A. Herman, L. Lalouat, K. D. Lee, J. Liu, K. Lodewijks, F. Mandorlo, I. Massiot, A. Mayer, J. Muller, P. Narchi, R. Orobtchouk, G. Picardi, P. Prodhomme, P. Rocai Cabarrocas, C. Seassal, C. Trompoukis, I. Gordon, and J. Poortmans, in: proceedings of 29th PV Solar Energy Conference and Exhibition – EUPVSEC, Amsterdam, The Netherlands, 30 sept.-4 oct. 2014, pages:1461–1469.
38. C. Trompoukis, A. Stesmans, E. Simoen, V. Depauw, O. El Daif, K. Lee, I. Gordon, R. Mertens, and J. Poormants, "Photonic nanostructures for advanced light trapping in silicon solar cells: the impact of etching on the material electronic quality," Phys. Status Solidi Rapid Res. Lett. **2015**, 10394 (2015).
39. M. Otto, M. Kroll, T. Kasebier, R. Salzer, A. Tunnermann, and R. B. Wehrspohn, "Extremelly low surface recombination velocities in black silicon passivated by atomic layer deposition," Appl. Phys. Lett. **100**(19), 191603 (2012).
40. G. Von Gastrow, R. Alcubulla, P. Ortega, M. Yli-Koski, S. Conesa-Boj, A. Fontcuberta i Morral, and H. Savin, "Analysis of the atomic layer deposited Al2O3 field-effect passivation in black silicon," Sol. Energ. Mat. Sol **142**, 29–33 (2015).

1. Introduction

The concept of thinning down the photoactive material as a path towards cost reduction has been driving research activities in the field of crystalline silicon (c-Si) photovoltaics (PV) for already more than a decade. As a result, significant theoretical and experimental advancements have been made, taking advantage of both computational and experimental capabilities, further pushing the limits of technological achievements. In particular, one issue of major importance is to tackle the incomplete absorption of light in thin c-Si slabs due to the fundamental optical properties of silicon, i.e. its high refractive index and its low absorption coefficient originating from its indirect band-gap. As a consequence, various theoretical optics concepts have been investigated and various top-down or bottom-up fabrication techniques have been employed for enabling advanced light trapping for c-Si solar cells.

Recent developments in the field of nanophotonics [1] have brought the manipulation of light using photonic nanostructures for PV into the spotlight, even though there were earlier ideas discussing the incorporation of a diffraction grating in a solar cell [2]. Analytical calculations and simulations [3–5] have shown that absorption enhancement beyond the commonly accepted Lambertian limit [6,7] is possible through the use of periodic photonic nanostructures. As demonstrated in these studies, thanks to the coupling of light into certain diffraction orders, absorption is strongly enhanced around resonant wavelengths. However, in this approach, the absorption enhancement surpasses the Lambertian limit only for particular wavelengths. In order to achieve a more broadband effect, one has to compromise the strict wavelength selectivity of the photonic nanostructures. Excellent broadband antireflection properties have been achieved for random surface textures with features smaller than the wavelength of light, commonly known as "black" silicon [8–10]. Although such small features influence the amount of reflected and transmitted photons, limited light trapping occurs resulting in insignificant absorption enhancement of long wavelength photons [9]. Therefore, such surface texture does not bring significant improvement on the light path enhancement aspect unless the feature size is increased so as to induce better scattering of light [11].

Somewhere between perfect order and complete randomness lies a recent approach based on introducing a certain degree of disorder. Various concepts have been proposed including an amorphous/short range order [12,13], a certain degree of perturbation on a periodic nanopattern [14] as well as a super-cell approach [15], all reporting in an absorption enhancement surpassing micron-scale textures and periodic wavelength-scale nanostructures. Additionally, the robust optical behavior of such disordered nanostructures with respect to light incident angle has been reported [16] and theoretical guidelines for optimal disorder

#251986 Received 15 Oct 2015; revised 25 Nov 2015; accepted 29 Nov 2015; published 11 Dec 2015

such as the importance of a high pattern area fill fraction have been given [17]. However, contrarily to periodic and random nanopatterns whose optical performance and fabrication techniques [9,18] have been extensively reported, either by low-cost top-down [19] or bottom-up approaches [20–22], the fabrication of disordered photonic nanostructures has so far been done by expensive techniques [14,15].

In this paper we report on the combination of a bottom-up technique, hole-mask colloidal lithography (HCL) [23], and silicon etching in order to enable the fabrication of disordered nanopatterns. Based on the fact that this technique presents multiple advantages such as versatility, simplicity and processing over large areas, it could offer a cost effective method for integrating advanced light trapping schemes in a solar cell fabrication flow [24]. The optimization of the process, with respect to both the colloidal lithography and silicon etching in order to achieve a controlled fabrication, is presented and the optical performance of the fabricated disordered nanostructures is discussed.

2. Experimental methods

In order to study the optical properties of the fabricated nanostructures, two substrates were used with different thicknesses: 700 µm thick c-Si wafers and 1.1 µm thin c-Si slabs bonded on glass [25]. On one hand, we consider the 700 µm thick c-Si wafers as semi-infinite since all the light entering the sample with a wavelength lower than 1050 nm will be absorbed with a near 100% probability before reaching the back side. This offers therefore the possibility to study only the light/matter interaction on the front interface between air and silicon (light in-coupling). On the other hand, the ultra-thin 1 µm c-Si slabs bonded on glass act as an asymmetric waveguide in the low absorption limit offering the possibility to investigate the light confinement (light-trapping). In order to focus only on the optical properties of the nanopattern and to avoid effects such as parasitic absorption (i.e. absorption occurring elsewhere than in the photoactive layer) or thickness variations due to conformity issues [26], no antireflection coatings (ARC) or metal back reflectors were used.

The fabrication of nanostructures with a short-range order was done by hole-mask colloidal lithography (HCL) [23]. The process building blocks, schematically shown in Fig. 1, include a) the adsorption of surface-charged polystyrene (PS) beads, b) the etch mask deposition, c) the beads removal and d) the pattern transfer by silicon etching. A triple layer consisting of PDDA (polydiallyldimethylammonium), PSS (poly(sodium 4-styrenesulfonate)) and ACH (aluminium chloride hydroxide) was deposited on top of the silicon surface. Afterwards, a colloidal solution consisting of negatively charged polystyrene (PS) beads was adsorbed on the surface. A range of PS bead sizes from 170 nm to 850 nm were used. The coexistence of repulsive inter-particle interactions and attractive bead-substrate interactions leads to the assembly of the beads into an amorphous array, i.e. with short-range order. In a subsequent step, an etch mask was deposited on top of the PS beads covered substrate (Fig. 1(b) and 1(c)). Thermally evaporated aluminum or silicon oxide films with a thickness of 50 nm were used as hard mask. After beads removal, a nanohole-patterned etch mask with a short-range order was obtained. Finally, silicon etching was done either by dry plasma or wet chemical anisotropic etching through the aluminum or silicon oxide etch mask, respectively. Fluorine-based plasmas in combination with oxygen (SF_6 / O_2) were used in order to etch silicon at low pressure. The chemical etchant for anisotropic etching was tetramethylammonium hydroxide (TMAH), 10% diluted in water, at 80°C.

#251986 Received 15 Oct 2015; revised 25 Nov 2015; accepted 29 Nov 2015; published 11 Dec 2015

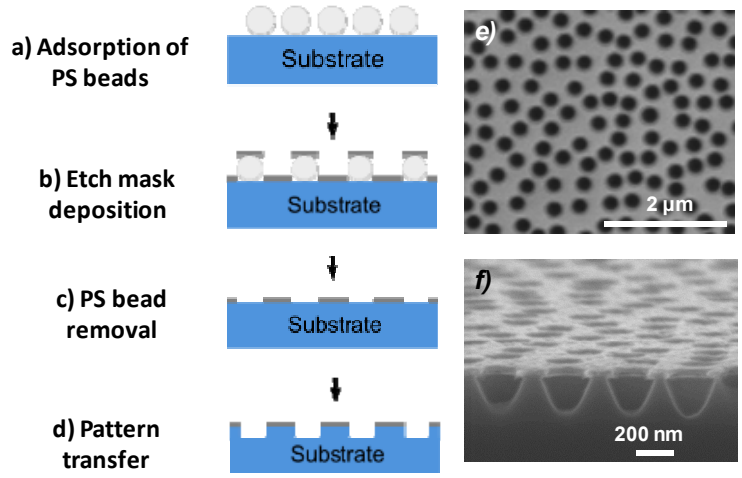

Fig. 1. (a-d) Schematic representation of the process flow. (e, f) scanning electron microscopy images of the nanostructures showing on (e) a top-view their distribution and on (f) a tilted view of their etched profiles.

The periodic photonic nanostructures used for comparison were fabricated by STU (simultaneous thermal and UV) nanoimprint lithography [27, 28]. The topography of the fabricated photonic nanostructures was characterized by scanning electron microscopy (SEM). Spectrally resolved reflectance (R(λ)) and transmission (T(λ)) measurements, with light impinging on the sample at near normal incidence and a measurement step of 10 nm, were performed using an integrating sphere in order to evaluate their optical performance (samples being positioned outside of the sphere). Absorption was then extracted as A(λ) = 100 - R(λ) - T(λ). For comparing the overall performance, the integrated values of reflectance were used as the figure of merit (between minimum and maximum values corresponding to the wavelength range where silicon absorbs, i.e. 300-1170 nm). They are the ratio of the number of reflected photons to the total number of incident photons over the wavelength range relevant for c-Si absorbance, taking into account the AM1.5 global tilt intensity distribution. The total number of reflected photons is given by:

$$\Phi_R = \int_{\lambda_{\min}}^{\lambda_{\max}} \frac{\lambda}{hc} \cdot S_{AM1.5G}(\lambda) \cdot R(\lambda) d\lambda \qquad (1)$$

where Φ_R is the integrated reflected photon flux (in units of number of photons/s·m^2), λ is the wavelength of light, h is Planck's constant, c is the velocity of light, $S_{AM1.5G}$ is the global tilt solar intensity distribution at the air mass of 1.5 and R is the measured reflectance value. The same formula can be used for estimating the number of absorbed photons (integrated absorption) by using the calculated absorption A(λ) values. For the case of the 700 µm thick c-Si wafers, the range of studied wavelengths was limited to 300-1050 nm (1050 nm being the wavelength of light right before reaching the back side of the 700 µm thick c-Si slab) when calculating the integrated values in order to correctly implement the concept of the semi-infinite slab and restrict the discussion only on the front interface between air and silicon.

3. Results and discussion

In this section, we discuss the essential parameters for the control on the nanopatterning technique. We present on one hand the bead distribution characterization and on the other hand the etched profile resulting from the transfer of the nanopattern on silicon. Finally, we

#251986 Received 15 Oct 2015; revised 25 Nov 2015; accepted 29 Nov 2015; published 11 Dec 2015

discuss the behavior of the fabricated disordered nanostructures with respect to light in-coupling (i.e. on 700 µm thick wafers) and light trapping (the case of 1 µm c-Si slab on glass).

3.1 Characterization of the beads distribution

The combination of two forces, i.e. bead-to-bead electrostatic repulsion and bead-to-substrate electrostatic attraction, defines the position of the beads. A good control on the process is needed in order to balance those two forces, avoid the agglomeration of the beads and achieve a short-range ordered array on the silicon surface. As shown in the top view SEM images of Fig. 2, a uniform distribution has been achieved for a wide range of PS bead sizes (from 170 nm to 850 nm) relevant for the specific application in wavelength-scale light trapping for c-Si.

SEM image analysis was then used to check the short-range order. The inter-particle spacing distribution can be characterized by extracting the nearest neighbor (NN) distance from the SEM image, i.e. the center-to-center distance between one given bead and its nearest neighbor. In the same fashion as the nearest neighbor distance, we have defined the 3 nearest neighbor (3NN) distance to take into account the inhomogeneities in the beads pattern. As shown in Fig. 2(b) for a size of 270 nm, the beads are arranged on the silicon surface following a Gaussian distribution. Moreover, we have calculated the inter-particle spacing distribution for different PS bead sizes by statistical analysis of the SEM image. We have then extracted the mean values of the NN and 3NN distances as the values corresponding to the peaks of the Gaussian fits in the case of the NN and 3NN distributions, respectively. As shown in Fig. 2(c), for all bead sizes, the average distance between two neighboring beads (center to center) is approximately twice their diameter.

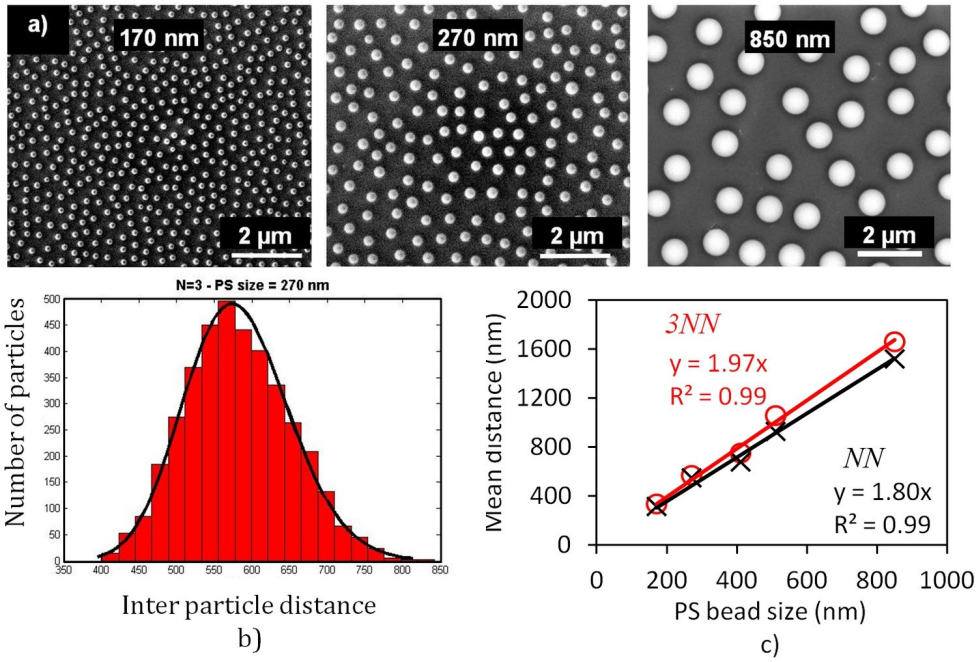

Fig. 2. Beads distribution analysis: (a) SEM image of the resulting bead distribution for bead sizes of 170, 270 and 850 nm, (b) 3 nearest neighbor distribution plot (red) with Gaussian fit (black curve) for the 270 nm bead size and (c) mean nearest neighbor (NN, black) and 3 nearest neighbor (3NN, red) values for various bead sizes.

#251986 Received 15 Oct 2015; revised 25 Nov 2015; accepted 29 Nov 2015; published 11 Dec 2015

3.2 Transfer of the pattern by silicon etching

In order to transfer the pattern from the etch mask to silicon, two techniques were used (dry and wet etching) targeting different hole profiles. It should be mentioned that we investigate two etching techniques due to the fact that wet etched nanostructures have been shown to enable higher minority carrier lifetimes compared to dry etched nanostructures when passivated by hydrogenated amorphous silicon [29]. Moreover, we target the fabrication of nanostructures with high area fill fractions, defined as the ratio of the area covered by holes over the total area, based on theoretical guidelines presented earlier [17].

After dry plasma etching, surface corrugations featuring etched holes with a parabolic U-shape were obtained. By tuning the plasma parameters, the hole diameter and the area fill fraction can be altered by an under-etch which is present during the dry plasma etching process (Fig. 3(a) and 3(b)). In fact, because of the chemical constituent of the etching mechanism, free fluorine atoms diffuse on the silicon surface and reach areas under the etch mask where they get adsorbed and desorbed along with silicon [30]. Therefore, starting from a bead size of 270 nm (red dot in Fig. 3(a)) and an initial area fill fraction of around 20%, the respective shape expansion (red arrows in Fig. 3(a)) due to long etch rates results in a higher final area fill fraction of 94%.

After anisotropic wet chemical etching, inverted nanopyramids are obtained on the silicon surface. Contrary to dry etching, high area fill fractions could not be achieved by increasing the etch time in order to achieve an over-etch. Therefore, a significant limitation arises highlighting the incompatibility between this colloidal lithography process and the anisotropic etching of silicon. This limitation is due to (i) the variable distance between nearest neighbors and (ii) the difference (~40 times) in the etch rates between the (100) and the (111) planes during anisotropic wet chemical etching [31]. It is well known that the area which is enclosed in the square that surrounds a certain corrugation, in our case a circle, is the area which is being etched. When two neighboring rectangles (defining the area to be etched) overlap, the final etched area becomes the new rectangle enclosing the two neighboring corrugations (Fig. 3(c)). Therefore, as shown in Fig. 3(c) and 3(d), neighboring nanostructures can merge and form large pyramidal or trapezoidal structures making the shape expansion for short-range ordered corrugations uncontrollable.

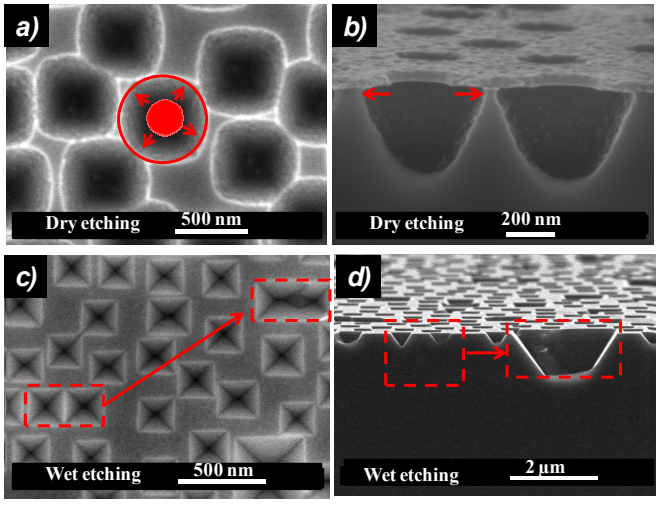

Fig. 3. Scanning electron microscopy images of (a, b) parabolic shaped nanostructures and (c, d) inverted nanopyramids after HCL. In (a) and (b), the arrows represent the under-etch which leads to an increased area fill fraction. In (c) and (d), the failing mechanism of merging neighboring corrugations due to the disordered distribution of PS beads leading to micron-scale features is highlighted.

#251986 Received 15 Oct 2015; revised 25 Nov 2015; accepted 29 Nov 2015; published 11 Dec 2015

In order to enable the fabrication of inverted nanopyramids with as high area fill fractions as possible, the initial bead inter-distance should be reduced as much as possible, so as to minimize the required over-etch. In order to make such a dense pattern, the repulsive force between the particles should be minimized. This can be done by adding ions, such as sodium chloride (NaCl), to the colloidal solution to increase the ionic strength of the solution and thus screen the electrostatic repulsive inter-particle interaction [32]. However, the repulsive and attractive forces should stay balanced so that the bead inter-distance distribution is not altered (and particularly so that aggregation is avoided).

The extent to which we can tune the achieved etched profiles so as to control the depth of the fabricated nanostructures is different for dry and wet etching. For the inverted nanopyramids, the depth and base are interlinked thus limiting the degrees of freedom on the achievable etched profile. On the contrary, more degrees of freedom exist in the case of the dry etching. The shape (depth and area filling fraction) of the dry etched nanostructures could be controlled, to a certain extent, by tuning the etching parameters such as power, pressure and oxygen concentration. However, careful tuning of the etching parameters is needed in order to balance the extent of the physical and chemical etching and achieve deep holes without losing in area fill fraction. The effect that the etched hole profile is expected to have on the performance of the fabricated nanostructures has already been investigated. In particular, it has been shown [33,34] that better optical performance is achieved by deeper surface corrugations. Moreover, as discussed in [35], the optimal set of parameters oscillates when scanning the individual parameters (period, depth etc) giving several local maxima of the achievable current for either shallow or deep corrugations, with good tolerance with respect to variations in the individual parameters.

3.3 Optical properties of the disordered nanostructures

3.3.1 Light in-coupling (700 μm thick wafers)

The light in-coupling behavior of the fabricated nanostructures with short-range order follows the same trends as in the case of the periodic nanostructures presented in [29].

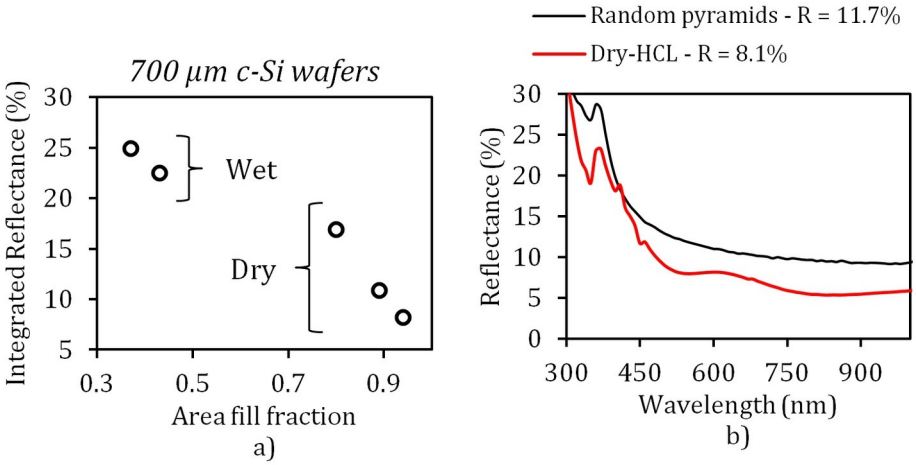

Fig. 4. Optical properties on 700 μm c-Si slabs: (a) integrated reflectance for various area fill fractions for Wet-HCL and Dry-HCL. (b) reflectance curve of the best achieved disordered nanopattern and benchmarking with state-of-the-art random pyramid texturing.

More precisely, as shown in Fig. 4(a), high area fill fractions result in better antireflective properties because of a gradual change in the refractive index between air and silicon. In the case of pattern transfer via dry etch (Dry-HCL), high area fill fraction and deep corrugations could be achieved which resulted in a low integrated reflectance of 8.1%. On the contrary, in

#251986 Received 15 Oct 2015; revised 25 Nov 2015; accepted 29 Nov 2015; published 11 Dec 2015

the case of pattern transfer via wet etch (Wet-HCL), where high area fill fractions could not be reached, the integrated reflectance remained high because of many flat areas in between neighboring surface corrugations and quite shallow structures. In both Wet-HCL and Dry-HCL cases, the higher the area fill fraction, the better the light in-coupling and therefore, the lower the integrated reflectance. The best antireflective performance is observed for the combination of 270 nm PS beads and dry etching which resulted in nanostructures having diameters and an average distance of corrugations around 620 nm. As shown in Fig. 4(b), the integrated reflectance of the best Dry-HCL (8.1%) is lower than the benchmark reflectance of state-of-the-art random pyramid texturing (11.7%). Besides the better absorption of the disordered nanopattern with respect to the random pyramid texturing, a better angular robustness [26] is an important added value which could contribute to an increased energy yield of a solar module.

3.3.2 Light trapping (1 µm-thin c-Si slab on glass)

In order to study the light-trapping properties of the disordered nanopattern, 1.1 µm-thin c-Si slabs were used. For the fabrication of the disordered nanostructures, PS beads with a size of 270 nm were used and various area fill fractions were obtained by tuning the etching parameters (SEM shown in Fig. 5(b)). It should be noted that we restricted the fabrication only to 270 nm beads since the combination of this size with the parameters of dry etching resulted in the best antireflective properties as discussed in the previous section (shown in Fig. 4(a)). The effect of the area fill fraction on the optical properties of the fabricated disordered nanostructures is shown in Fig. 5(a): the higher the area filling fraction, the higher the absorption. This trend was also theoretically shown in [17] for disordered nanopatterns on c-Si slabs with similar thicknesses as the one used here.

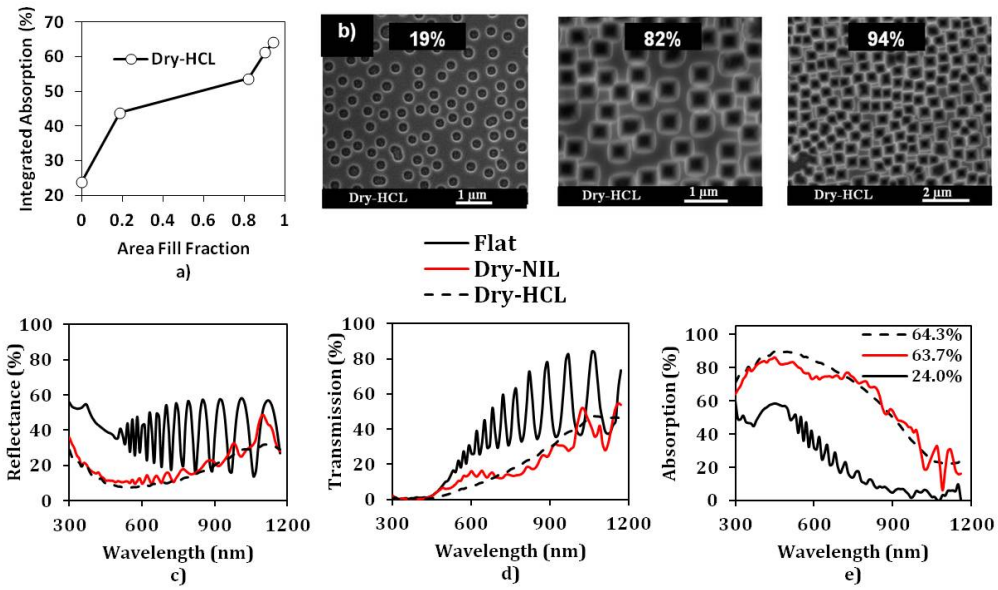

Fig. 5. Optical properties on 1.1 µm c-Si slab on glass: (a) integrated absorption for various area fill fractions of the disordered nanopattern, (b) SEM images of disordered nanostructures with varying fill fraction, (c - e) transmission, reflectance and absorption spectra of flat, periodic and disordered nanostructures.

We first compare the optical performance (transmission, reflection and absorption spectra) of the disordered nanostructures and the flat slab (Fig. 5(c), 5(d) and 5(e), respectively). For a flat slab of a thickness of 1.1 µm, light impinging on the device does not efficiently couple to

#251986 Received 15 Oct 2015; revised 25 Nov 2015; accepted 29 Nov 2015; published 11 Dec 2015

quasi-guided modes, and therefore absorption remains low (24%). The integration of the wavelength-scale disordered nanostructures leads to the excitation of guided modes, thus resulting in an absorption enhancement compared to the flat slab. As shown in Fig. 5(e), the absorption increased from 24% for the flat slab up to 64.3% for the disordered nanopattern. Focusing on the photons which do not reach the back side of the slab, i.e. for photons with wavelengths shorter than 550 nm (this wavelength corresponds to a penetration depth in silicon of less than 1 μm, also seen in Fig. 5(d) where the transmission through the flat slab starts for this wavelength) the absorption is enhanced due to a gradual change of refractive index from air to silicon and therefore better light in-coupling. Moreover, a better light confinement compared to the flat slab is achieved thanks to the disordered photonic nanostructures. This becomes obvious for photons with wavelengths longer than 550 nm where the absorption is strongly enhanced. Finally, it should be highlighted here that the Fabry-Perot resonances seen for the flat slab fade away for the disordered nanopattern.

Additionally, we compare the best absorption spectrum of the fabricated disordered nanopattern to the absorption spectrum of a periodic nanopattern. The purpose here is to highlight the similarities and differences in the optical performance of the two experimentally fabricated nanopatterns, rather than concluding on which nanopattern is the best, a question which normally emerges when comparing a periodic and a disordered nanopattern [36]. The periodic nanostructures are fabricated by nanoimprint lithography and dry etching (Dry-NIL) and they have geometrical dimensions (pitch of 650 nm, diameter of 570 nm and a depth of 500 nm) which are close to the disordered pattern (3NN of 620 nm, diameters ranging between 550 and 650 nm and a depth of 500 nm). On one hand, the periodic and disordered nanostructures have similar light in-coupling behavior. This is due to the similar hole shape and dimensions for the two nanopatterns which enables a similar gradual change of the refractive index. On the other hand, for ordered structures the Fourier spectrum is well defined, which enables the efficient coupling of light into specific wavelengths. For the disordered structures, a richer Fourier spectrum is obtained, which results in an increasing number of accessible diffraction orders and therefore a higher density of photonic states [13–15]. In particular, the peaks seen for the periodic nanopattern because of the resonant modes, broaden spectrally for the disordered nanopattern revealing an overlap of modes. As a result, a smoother absorption spectrum is obtained for the disordered patterned. Overall, for the 1.1 μm crystalline silicon slab on a glass carrier, the disordered nanostructures result in an integrated absorption (64.3%) which is comparable to the integrated absorption for the periodic nanostructures (63.7%).

4. Conclusions

We report on the fabrication of disordered photonic nanostructures following a bottom-up approach combining colloidal lithography and (dry or wet) silicon etching. We have shown good control of the short-range ordered colloidal pattern for a wide range of bead sizes from 170 to 850 nm relevant for photon wavelength-scale texturing. The pattern's inter-particle spacing follows a Gaussian distribution and the average distance between two neighboring beads (center to center) is approximately twice their diameter. We have investigated the case of inverted nanopyramids obtained by wet chemical anisotropic etch, which has a higher potential for good surface passivation. However, so far, the optical performances of disordered wet etched nanostructures are limited by the low values of filling fractions that can be reached. This limitation could be circumvented by increasing the density of the initial colloidal pattern or by using a more isotropic wet etch process in order to improve the control of the under-etch. Regarding the short-range ordered arrays of U-shaped parabolic holes obtained by dry etching, we have demonstrated experimentally that they outperform the micron-scale random pyramid texturing. When integrated in a 1.1 μm thin crystalline silicon slab bonded on glass, the absorption is enhanced from 24.0% for the flat slab up to 64.3% for the disordered nanopattern. Moreover, the broadening of resonant modes seen for the

#251986 Received 15 Oct 2015; revised 25 Nov 2015; accepted 29 Nov 2015; published 11 Dec 2015

disordered nanopattern offer a more broadband light confinement compared to a periodic nanopattern. As mentioned earlier, the results presented in this study are related to nanopatterned samples which did not include any additional light trapping related layers (mainly ARC or metal back reflector) in order to avoid effects such as parasitic absorption (i.e. absorption occurring elsewhere than in the photoactive layer) or thickness variations due to conformity issues [26]. However, those layers are normally included in a solar cell stack. It should be mentioned that the broadband antireflection effect and light trapping properties of the fabricated nanopatterns are superimposing with the antireflection effect from an ARC which targets a specific wavelength. Interestingly, tailoring the optical properties by optimizing the pattern parameters can also lead to new degrees of freedom when designing the full cell stack of a photonic-assisted solar cell [37]. These two effects could be combined to design a solar cell with better overall optical performance and/or lower cost. For instance, the incorporation of a thinner ARC or even no ARC at all (currently SiNx as an ARC is one of the most expensive steps during the fabrication of a state of the art solar cell) could be envisaged. The glass and encapsulating material could also offer a combined gradual change of refractive index enabling either thinner or no ARC. Regarding the material quality after nanopatterning, dry etching has been shown to result in low minority carrier lifetimes due to i) a high density of dangling bonds and ii) the presence of sub-surface defects [38]. However, recent developments with atomic layer deposition of aluminum oxide (Al_2O_3) have enabled reaching high lifetimes. In particular, surface dangling bonds can be efficiently passivated with Al_2O_3 [39] while the formed field-effect passivation mechanism depletes the nanopattern from minority carriers [40].

We foresee that the presented, potentially low-cost bottom-up nanopatterning process opens perspectives towards the integration of advanced light-trapping schemes in thin solar cells owing to its simplicity, versatility and the degrees of freedom it brings. Therefore, combining recently developed surface passivation schemes and disordered nanopatterns for advanced light management as presented here opens the way towards efficient photonic-assisted thin solar cells.

Acknowledgments

The work was supported by the European Union's Seventh Programme for research, technological development and demonstration under grant agreement No 309127, PhotoNVoltaics (Nanophotonics for ultra-thin crystalline silicon photovoltaics). The authors would like to thank the partners of PhotoNVoltaics and Aimi Abass for fruitful discussions.

#251986 Received 15 Oct 2015; revised 25 Nov 2015; accepted 29 Nov 2015; published 11 Dec 2015